JCTC Journal of Chemical Theory and Computation

A Quantum Chemical Interpretation of Compressibility in Solids

J. Contreras-García,[†] P. Mori-Sánchez,[‡] B. Silvi,[§] and J. M. Recio*,[†]

MALTA-Consolider Team and Departamento de Química Física y Analítica Universidad de Oviedo, E-33006 Oviedo, Spain; Department of Chemistry, Duke University, Durham, North Carolina 27708; Laboratoire de Chimie Théorique, Université Pierre et Marie Curie, F-75252 Paris, France

Received May 5, 2009

Abstract: The ability of the electron localization function to perform a partition of the unit cell volume of crystalline solids into well-defined, disjoint, and space-filling regions enables us to decompose the bulk compressibility into local contributions with a full chemical meaning. This partition has been applied to a set of prototype crystals of the chemical elements of the first three periods of the periodic table, and the equations of state for core, valence, bond, and lone electron pairs have been obtained. Solids are unequivocally classified into two groups according to their response to hydrostatic pressure. Those with sharing electrons (metals and covalent crystals) obey a simple relationship between the average valence electron density and the zero pressure bulk modulus. The stiffness of the closed-shell systems (molecular and ionic solids) is rationalized resorting to the Pauli principle. Overall, the results clearly correlate with chemical intuition: periodic trends are revealed, cores are almost incompressible and do not contribute appreciably to the macroscopic compressibility, and lone pair basins are rather easier to compress than bond basins.

1. Introduction

Since the beginning of the 20th century,[1,2] many phenomenological equations and theoretical models have been proposed with the aim at explaining and predicting the compressibility of crystalline materials. Standard equations of state nowadays in use for solids have their roots in these pionner works. State of the art developments (see ref 3 and references therein) highlighted the importance of finding correlations between the systematic behavior of the zero pressure bulk modulus (B_0) along the periodic table with the microscopic properties of chemical elements. Interestingly enough, Gilman[3] invoked the core−valence separation to emphasize that the average valence electron density (the ratio between the valence electron population and the corresponding volume) is a key parameter that shows an interesting correlation with B_0 in simple solid materials.

Though it is clear that the macroscopic compressibility of a crystal is ultimately determined by its chemical bonds and valence electrons, no systematic and quantitative account of this correlation in quantum chemical terms has been given so far. This is partially due to the need of an unambiguous partition of the unit cell volume into well-defined, disjoint, and space-filling regions. It is our point of view that such a partition, of the 3D space into core and valence shells with a subsequent division into regions associated with bond and lone electron pairs, can contribute to a global understanding of the compressibility of solids. In order to properly define the local compressibilities of the subregions, the volumes and charge populations of these basins have to be accessible. The topology of the electron localization function (ELF),[4] which is derived from the conditional pair electron density and is related to its Laplacian, provides such a partition, and the integration of space and charge within the above basins allows us to assign volumes and electron populations to each

* Corresponding author. Fax: (+34)985 103125. E-mail: mateo@fluor.quimica.uniovi.es.

[†] Universidad de Oviedo.

[‡] Duke University.

[§] Université Pierre et Marie Curie.

10.1021/ct900224w CCC: $40.75 © 2009 American Chemical Society
Published on Web 07/10/2009

of them. Thus, the equations of state and the average electron density for all these chemical regions will be at hand.

In this paper, our aim is to illustrate how the information contained in crystalline wave functions can be quantitatively translated to the macroscopic compressibility in terms of chemical (core, valence, bond, and lone pairs) contributions. Our target systems are the crystalline phases of most of the chemical elements located in the first three rows of the periodic table. We have computed volumes and charges at different pressures for all the regions or basins in which the ELF divides their respective unit cells. Systematic trends have been recovered, and general trends will be proposed. The validity of the empirical relationships based on the average electron density of pressure sensitive regions, as proposed by Gilman,[3] is hereby tested by means of the quantitatively and theoretically grounded analysis of valence properties provided by the topological analysis of the ELF.

We organize the rest of the paper as follows. In Section 2, the ELF basic concepts and computational details are briefly summarized. Section 3 deals with the pictures that ELF provides to understand how pressure affects solids of different chemical bonding nature. Section 4 contains the results of our analysis on the response to pressure of the solids of most of the chemical elements with atomic numbers up to $Z = 20$. The main conclusions are gathered in Section 5.

2. Theoretical Background and Computational Details

2.1. Summary of ELF Concepts. Becke and Edgecombe[4] introduced the ELF as a local measure of electron localization. Its core, χ, is formulated in terms of the conditional probability of finding one electron in the neighborhood of another one of the same spin, rescaled with respect to this probability in a uniform electron gas value of the same electron density. In order to have a direct relationship between the function and localization values of ELF are constrained between 0 and 1 by a *cosmetic* Lorentzian transformation $\eta = 1/(1 + \chi^2)$, so that when η tends to 1, parallel spins are highly improbable (and paired or lone electrons are, therefore, highly probable), whereas η tends to 0.5 in those regions where the electrons follow the homogeneous electron gas distribution.

A detailed presentation of the topological features of ELF is given elsewhere.[5] We recall here that zero flux surfaces of the ELF gradient enclose 3D regions or basins that can be associated with electron shells, bonds, or lone pairs. The power of the ELF partition in the case of crystalline systems lies in the fact that these basins are finite, disjoint, and space filling, which means that the macroscopic volume is recovered when all of them are added together. Each of these basins contains a maximum or attractor of ELF, and between two of these attractors we find a first-order saddle point whose ELF value provides information about the interaction between the corresponding basins. If the ELF value at this point is very low, then electron delocalization between those basins is not expected. In practical terms, it is the same as to say that there will not be charge flow from one basin to the other basin when pressure is applied. The opposite is expected if the ELF value is high. These first-order saddle points are called bond interaction points or *bips*. To facilitate the identification of these relevant relationships, it is interesting to track the ELF values along the path connecting two atoms of the unit cell. This plot highlights the approximate position of the attractors and the *bips* of the system revealing the atomic structure in shells, the presence of bonds and lone pairs, and how the different basins are interconnected. In the Section 2.2, ELF profiles for different bonding patterns will be analyzed.

2.2. Computational Parameters. In order to build the electron localization function for a given crystal structure, it is necessary to carry out all-electron calculations. We have followed first-principles methodologies based on the density functional theory as implemented in VASP and CRYSTAL98 packages.[6,7] Since it is known to affect to a little extent the results provided by the topological analysis of ELF,[8] the choice of functionals was mainly dictated by the proper computational convergence of the crystalline phase. As a general guideline, delocalized structures, such as metals, were calculated under the local density approximation,[9] whereas the Perdew−Wang functional[10] was preferred for the electronic description of ionic and molecular solids. Basis sets have been taken from literature sources,[11,12] and standard computational parameters have been checked to ensure convergence in the calculations. We have computed with the VASP code the energy and the electronic structure at different unit cell volumes of the crystalline phases of most of the chemical elements with atomic numbers up to $Z = 20$. The energy−volume data for each of the compounds provide the necessary input to evaluate the corresponding equation of state (EOS) parameters: the equilibrium volume (V_0), the bulk modulus (B_0), and its first pressure derivative (B_0') evaluated at zero pressure. Single point calculations at each of the full optimized structures calculated with VASP were later performed with CRYSTAL98 to obtain the total electron density in the unit cell from all-electron calculations.

An extension of our CRITIC code[13] has been recently developed to carry out a thorough topological analysis of the ELF in crystals.[14−17] Making use of automated and efficient recursive algorithms, it is able to provide an accurate analysis and characterization of critical points of the ELF topology in the unit cell. Basin volumes (v) and charges (q) are calculated by integrating the appropriate density operators and recovering the unit cell value. A thorough description of the new abilities of the CRITIC code in the studies of the ELF topology in crystals is given elsewhere.[17]

For each of the crystalline phases under study, quantitative data of the basins response to pressure (p) are obtained evaluating volume basins (v) at different pressures according to the previous computed EOS of the corresponding crystal. Using standard analytical EOS functions as the Vinet one,[18] fittings to the sets of (v, p) points provide EOS parameters for each basin. In this way, we compute zero pressure basin volumes (v_i) and basin compressibilities (k_i). It now becomes interesting to find out that the macroscopic compressibility (k) of the crystal can also be expressed as a sum of contributions from these chemically meaningful basins:

$$\kappa = -\frac{1}{V}\frac{\partial V}{\partial p} = \sum_i f_i \kappa_i \quad (1)$$

where $f_i = v_i/V$ is the fractional occupation volume of the i-th basin. This equation holds if we keep the same formal definition for the basin compressibility as for the bulk, $\kappa_i = -(1/v_i)(\partial v_i/\partial p)$, and we apply the volume additive equation $V = \sum_i v_i$.[19,20] Here V and v_i refers to a formula unit in the cell. Thus, not only basin volumes and charge populations are additive but compressibilities too, which leads to the potential rationalization of the macroscopic response of solids to pressure in quantum chemical contributions.

3. Differential Behavior of Electron Pairs under Pressure

Let us consider the simple schemes of bonding patterns present in solids as depicted in Figure 1. The universal binding energy relation (UBER) model[21−23] establishes correlations between the electron density, bond strength, and bulk modulus of materials (see also ref 3). Considering these works, we can assume that regions with low average electron density are the natural candidates to be more affected by pressure. According to this chemical knowledge (and also to our quantitative analysis below), these regions can be clearly identified with arrows in each of the bonding schemes of Figure 1. If we move now to the ELF 1D profiles (Figure 2), it is found that, in all cases, these regions correspond to the basins with lower ELF values and, more specifically, the zones of these basins with the steepest ELF descent.

It is worth describing in detail these ELF profiles, and we take as a first example that of the diatomic N_2 molecular crystal (see Figure 2b). We only refer to the left-half of the plot since the curve is symmetric with respect to $R(N_2 - N_2) = 0.5$, where R is a reduced length coordinate. The two highest maxima are associated with the K-shells ($1s^2$ electrons) of the two N atoms. Between these two peaks, there is another peak identifying the highly localized electrons corresponding to the N_2 triple bond. For our purposes, the most interesting features appear in the regions of the ELF profile the arrows are pointed to. These are the basins of the lone pair electrons, which spread out toward the other N_2 molecule. A first-order saddle point is found between them at $R = 0.5$, and the ELF value at this point is negligible. This reflects the description of the solid with strongly orthogonalized molecular-like (N_2) wave functions,[24] which results in the absence of charge flow between N_2 molecules as pressure is applied: Pauli prevents the occurrence of intermolecular overlaps. The same happens in the mono-atomic Ne crystal and in between Na^+ and Cl^- in NaCl.

For all these situations, we have found an interesting result: only the outermost part of the pressure active basins, starting at the most external maximum of the ELF profile, is compressed. This can be interpreted as the result of the Pauli principle that prevents electron mixing with the core as well as with other units. Hence, on the one hand, a minimal distance between nonorthogonalized orbitals is preserved, and the compression does not affect the ELF well. On the other hand, the core structure is also maintained so that the only

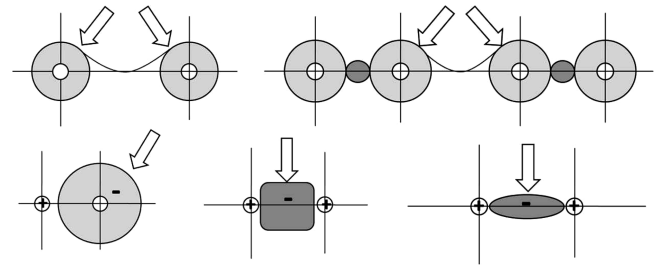

Figure 1. Bonding patterns in solids. From left to right and up to down: rare-gas monatomic, molecular diatomic, ionic, covalent, and metal. Arrows point to pressure sensitive basins. Dark regions stand for shared electrons, lighter ones for unshared electrons, and white ones for core electrons.

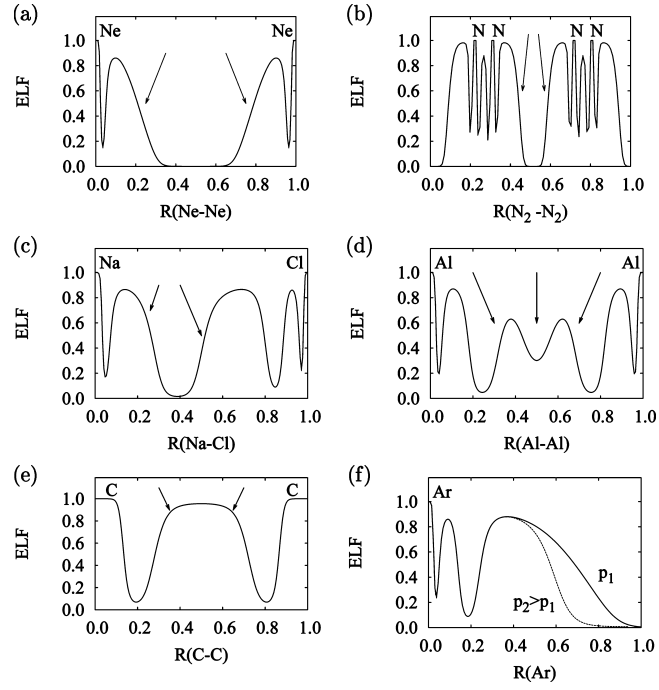

Figure 2. ELF profiles along the bonding path in solids: (a) rare-gas monatomic (Ne), (b) molecular diatomic (N_2), (c) ionic (NaCl), (d) metal (Al), and (e) covalent (C-diamond). ELF profiles, (f), for solid Ar at two pressures (p_1 and p_2). Arrows point at pressure sensitive basins. R is a reduced (relative) coordinate.

part of the atom that can subsume the pressure is the localized valence. Furthermore, due to the monosynaptic (they belong to only one nucleus) nature of these basins, the only part that is affected is the tail, as illustrated in Figure 2f, where the 1D ELF profile for Ar is plotted at two different pressures. The valence electron density in these closed shell systems surrounds the core with a radial distribution that is not at all uniform. The average electron density is much higher in the inner region of the lone pair basin than in its tail, and therefore, it is this part of the basin which is essentially affected by pressure. In addition, we should bear in mind that these closed-shell and lone pair basins contain electrons of the same spin, and again, Pauli repulsion makes their compression difficult.

As regards metals and covalent solids, the corresponding 1D ELF profiles clearly illustrate the electron shell structure of the atoms (high ELF values for the K-shell in C-diamond

Table 1. Zero Pressure Properties of Bulk and Basins of the Crystalline Phases for Most of the Elements with Atomic Numbers up to $Z = 20$ According to Our Calculations[a]

				core		valence		bond		lone pair		
E	SG	V_0	B_0	ρ_i	f_i	ρ_i	f_i	ρ_i	f_i	ρ_i	f_i	$B_{0,i}$
He	$Im\bar{3}m$	34.71	0	–	–	0.0085	1.000	–	–	–	–	–
Li	$Im\bar{3}m$	20.37	13.6	0.302	0.049	–	–	0.007	0.951	–	–	13.5
Be	$P6_3/mmc$	7.91	121.0	0.477	0.081	–	–	0.039	0.919	–	–	108.4
B	$R\bar{3}m$	7.32	200.0[b]	0.326	0.172	–	–	0.055	0.828	–	–	–
C	$Fd\bar{3}m$	5.71	442.8	2.637	0.021	–	–	0.104	0.979	–	–	445.4
N_2	$Pa\bar{3}$	55.21	62.4	4.634	0.002	–	–	0.066	0.142	0.020	0.855	54.8
Ne	$Fm\bar{3}m$	24.26	3.1	18.819	0.001	0.048	0.999	–	–	–	–	4.9
Na	$Im\bar{3}m$	37.10	7.0	0.470	0.083	–	–	0.005	0.917	–	–	8.5
Mg	$P6_3/mmc$	22.84	36.1	0.684	0.094	–	–	0.015	0.905	–	–	32.6
Al	$Pm\bar{3}m$	20.41	57.5	0.955	0.073	–	–	0.026	0.927	–	–	52.7
Si	$Fd\bar{3}m$	19.72	97.1	1.417	0.053	–	–	0.031	0.947	–	–	92.3
P	$Cmca$	18.98	58.9	2.061	0.026	–	–	0.027	0.974	–	–	58.6
Cl_2	$Cmca$	45.55	24.5	4.519	0.029	–	–	0.125	0.075	0.032	0.897	26.6
Ar	$Fm\bar{3}m$	39.37	0.7	6.033	0.006	0.030	0.994	–	–	–	–	0.3
K	$Im\bar{3}m$	70.88	4.7	0.150	0.238	–	–	0.002	0.762	–	–	4.5
Ca	$Fm\bar{3}m$	42.66	17.6	0.272	0.232	–	–	0.008	0.768	–	–	17.1

[a] E and SG stand for elements and space group, respectively. Volume (V_0) is in Å^3, bulk modulus for crystals (B_0) and for the basin with lowest ρ_i ($B_{0,i}$) are in GPa, average electron density (ρ_i) is in number of electrons per bohr,^{3} and volume occupation fraction (f_i). [b] Approximated from theoretical results of ref 25.

and for the K- and L-shells in Al) with bonding basins between them marked with the *pressure* arrows. In both cases, the valence basins are shared between two (or more) atoms so that both the ELF and density have high values along the bonding direction and both contours of the basin are subject to compression. Furthermore, since these basins feel several strong potentials from neighboring atoms, they are confined to smaller regions of space that, obviously, lead to smaller compressibilities. The high ELF values of the bonding basin in C-diamond reveal electrons highly localized with directional C−C bonds, whereas in Al, lower ELF values are associated with electrons delocalized among different bonding basins yielding a minimum in this 1D profile (see Figure 2d and e). Notice that the charge population, the average electron density, and the ELF values are lower in metals than in covalent bond basins since, in metallic elements, the number of valence electrons (up to three) is also lower, and the valence electrons are not completely paired. Moreover, the radial distribution of the electron density inside these basins is much more uniform than in the closed-shell systems, and we can think that all the electrons within the bonding basin are affected by pressure. The saddle point between the bond basin and the L-shell in Al has a low but not negligible ELF value that allows some charge flow between these basins as pressure is applied, leading to contributions from the outer core to the macroscopic compressibility. In fact, it is a common feature that the saddle point ELF value raises, and the ELF values in the bonding basin decrease with pressure, leading to a greater delocalization of the electron density.[16] These features are in contrast with the static picture drawn from molecular and ionic crystals, where *bip* ELF values are low and the contribution of electron delocalization between basins is negligible.

We conclude that there exists two main classes of compounds as far as the effect of pressure is considered. On the one hand, metal and covalent crystals (from now on called *type A* solids) are mainly affected by strong forces. On the other hand, molecular and rare-gas solids (from now on called *type B* solids) are characterized by the presence of electrons belonging to just one atom and are stabilized by weak interactions. Whereas in *type A* systems, the increase of interelectronic repulsions correlates with the material stiffness, *type B* solids can be seen as closed shell systems in which the underlying compression mechanism arises from the resistance to overlapping imposed by the Pauli principle.[3] The fact that their cohesion energy, unlike in *type A* solids, increases with atomic size constitutes a natural proof of the different forces at work.

4. Chemical Contributions to Compressibility in Solid Elements of the s and p Blocks

Crystallographic as well as bulk and basin EOS parameters are collected in Table 1. This table also contains the average electron density and the volume occupation fraction of each of the basin types in which the corresponding unit cells of the solid elements of the s and p blocks are divided. Preliminary results for core, bond, and lone pair compressibilities of some elements have been published elsewhere.[14] In Figure 3, we have used B_0 calculated values from Table 1 to plot the inverse of the bulk compressibility, along with the inverse of the compressibility of the basin more sensitive to pressure in each crystal.

The first question we would like to address is how the bulk compressibility compares with the compressibilities of the different basins that result from the ELF partition. It can be seen from eq 1 that two factors determine the contribution of the different basins to the total crystalline compressibility: on the one hand, the relative volume and, on the other hand, the basin compressibility. In all cases, and due to both factors, it is always possible to identify just one ELF valence basin for each crystal, as the basin that controls the pressure response of the crystal. This is apparent in Figure 3, where it is illustrated that not only the bulk modulus of each crystal,

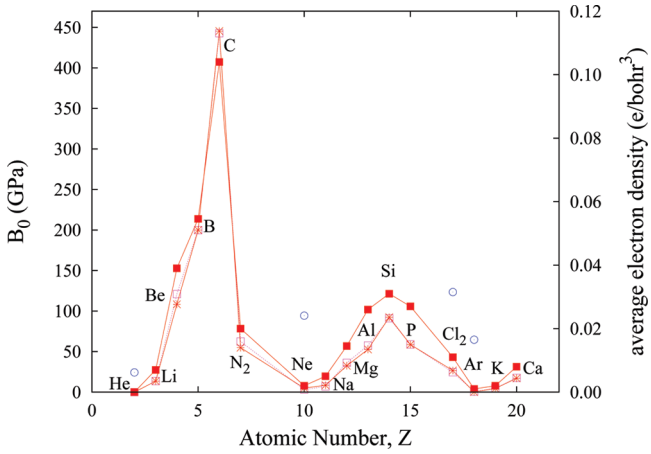

Figure 3. Dependence on the atomic number of bulk (empty squares) and valence basins (stars) compressibilities for most of the solid elements of the s and p blocks with $Z < 20$. Computed average electron densities of these basins (filled squares) are also included using the right *y* scale. Empty circles stand for uncorrected electron densities of He, Ne, Cl_2, and Ar.

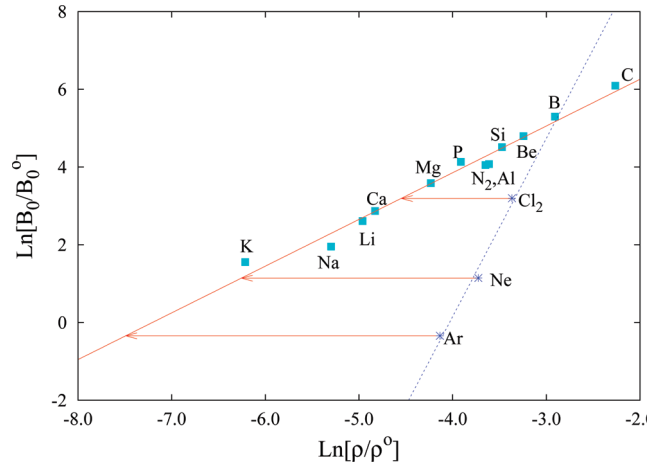

Figure 4. Linear fit showing the correlation between logarithms of zero pressure bulk modulus and logarithms of the average electron density of the *controlling* basin for *type A* solids. Missfitting to the general behavior is highlighted for *type B* solids with stars and a dotted line. B_0^o (1 GPa) and ρ^o (1 e/bohr^3) allow to remove dimensions in the corresponding ln functions.

and that of the *controlling* basin, follow the same periodic trend but also their absolute values are very similar. This reflects the fact that compressibility is a chemical property originated by valence electrons that are clearly identified by the topological partition of the ELF.

As we go from group I to VIII, we observe changes in the nature of that valence basin representing the main contribution to the bulk compressibility. It is first associated with a metallic bond basin (k_i in Li is 7.41 $\times$ 10^{-2} GPa^{-1}, and the calculated crystal value is 7.35 $\times$ 10^{-2} GPa^{-1}), then goes to a covalent bond basin (k_i in diamond C is 2.75 $\times$ 10^{-3} GPa^{-1} and k is 2.39 $\times$ 10^{-3} GPa^{-1}), then to a lone pair basin (in N_2 k_i is 1.82 $\times$ 10^{-2} GPa^{-1} and k is 1.60 $\times$ 10^{-2} GPa^{-1}), and ends with a closed-shell valence basin (in Ne k_i is 2.04 $\times$ 10^{-1} GPa^{-1}, and the bulk value is 3.18 $\times$ 10^{-1} GPa^{-1}). Under the ELF framework, this trend clearly recovers the decreasing connectivity of valence electrons along the periodic table. Metallic valences are in one extreme: in metals, the valence basins are located in the interstitial sites where they often form multicenter bonds; they are followed by prototypical two center two electron covalent bonds; lone pairs, which belong to just one center come next; and rare-gas solids, where all electrons are core-like, in the end. Overall, the contribution from the K-shell cores of these elements is almost negligible since their average electron density is very high, and strong forces are acting within them. Similar results are obtained from the analysis for the calculated elements of the second and third periods.

The correlation between the compressibilities of the crystals and the valence basins calls for a relationship similar to the ones derived in other theoretical and phenomenological models[3,25] but involving, in our case, the average electron density of their respective valence basins. It is graphically illustrated in Figure 4, where a standard plot of the logarithms of the computed crystalline B_0 values versus the logarithms of the average electron densities of the *controlling* basins are displayed. Successfully, the computed average electron density of the most sensitive ELF basin in each of all the studied *type A* crystals is very well described with a single linear function. The calculated slope (1.20) is very close to the value (1.26) reported by Gilman using the valence average electron density in elements of groups I−IV.[3] Notice also that the reference state (B_0^o) in Gilman's plot is 1 Mbar. We should stress that, in our case, B_0 values come from the first-principles total energy calculations and the average electron densities from the partition induced by the ELF topology. It is remarkable that, in the pioneer work of Richards[1] with experimental data of more than forty elements, an equivalent plot to the one drawn here would have a slope of 1.25. A linear behavior (slope is equal to 1) is obtained for families of compounds under the so-called B_0-V_0 inverse relationship proposed by D. L. Anderson and O. L. Anderson.[26] This kind of phenomenological expression has become very popular,[27] and identifies the formula unit volume as one decisive parameter to carry out correlations with the isotropic compression of solids. In our study, volume is subsumed in the average electron density of the *controlling basin*, which turns out to be a more general parameter to describe this behavior. Our results also reveal the ability of these valence basins more sensitive to pressure to enclose the periodic behavior of solid elements under pressure. Figure 3 shows the accuracy of this approximation, where the parameter ρ is able to recover the periodicity of the bulk modulus in *type A* solids.

As far as *type B* solids are concerned, when the electron density of their valence pressure active basins is displayed (empty circles in Figure 3), the periodic trend is broken. This behavior also appears in Figure 4, where the arrows indicate how far closed-shell crystals lay from the quasi-linear $B_0-\rho$ trend. Note that a different slope is expected for this *type B* solids (dotted line in Figure 4). As we have discussed in Section 3, the reason behind the different behavior exhibited by *type B* solids relies on the different character of the forces that are acting on their valence basins when pressure is

applied, which clearly do not follow a simple relationship with the electron density. *Type B* solids do not present basins with sharing electrons, and it is the average electron density of this kind of basins the one that correlates with B_0. Nevertheless, it might be interesting to have for this *type B* solids an *effective* average electron density equivalent to the one observed in *type A* systems. If we introduce B_0 values of *type B* solids in the linear fitting expression obtained for *type A* solids, we obtain the *effective* average electron density for these systems, as pointed by the tips of the arrows in Figure 4. These *effective* electron densities for *type B* solids recover a correct picture regarding the periodical trend collected in Figure 3.

Graphical inspection of Figure 3 also reveals that the trends both along the periods and down the families are qualitatively reproduced. In fact, since the valence is conserved down the families, dropping the electronic saturation of the *controlling* basin becomes, in most cases, a reasonable approximation, so that a qualitative analysis could be made only in terms of the cell volume of the *controlling* basin (see Table 1). Given the fact that the volume increases as we go down, it is expected higher compressibilities for the heavier elements of the family. This is easily checked down the alkalines series Li−Na−K, where the volume increases from 20.4 to 70.9 $Å^3$ and the bulk modulus decreases from 13.6 to 4.7 GPa. However, there are some cases where the cell volume turns out to be a deficient descriptor and resorting to the average electron density of the *controlling* basin becomes necessary in order to understand the exhibited periodicity. This is, for example, the case with Si and P. In spite of having nearly the same atomic volume, the greater number of valence electrons in Si results in a much lower compressibility. It should be noted that some general assumptions can still be made along the periods related to the nature of the compounds. The greatest volumes, along with the weak long-range forces, involved in both molecular crystals and rare-gas solids give rise to the most compressible solids. In the other extreme, compact covalent bond basins are the most difficult to compress, since they have the smallest *controlling* basins.

Finally, we would like to point out that the correlations we have shown between B_0 and the average electron density of valence basins have been computed after an exhaustive partition of the unit cell space into basins as induced by the ELF topology. Similar topological analyis under the framework of Bader's formalism yields valuable information in the case of closed shell systems, as alkali halides or oxide and selenide spinels,[19,28] but it is not able to go inside the chemistry of the different types of bonding patterns shown in the systems explored here. In the case of many of the solid phases of these chemical elements, the average valence electron density can be computed from the difference between unit cell (and total number of electrons) and core volumes (and core electron populations). Core volumes in crystals are available for some elements from X-ray scattering experiments (see pages 116−117 in ref 3) and can be also estimated from ELF topological analysis in atoms under the reasonable assumption of negligible distortion of the inner electron shells when atoms go from a gas to a crystalline phase. In fact, atomic core volumes and electron populations have been previously computed by Kohout and Savin[29] and Matito et al.[30] after much less expensive ELF topological analyses in atomic systems. We have checked that a good qualitative agreement with our results are obtained when the numbers from these calculations are used to display the periodic trends analyzed in the present study.

5. Conclusions

We would like to highlight the success of the underlying formulation behind our approach when looking for a comprehensive understanding of the crystalline response of elements to hydrostatic pressure. Our analysis provides a deeper insight into the periodicity of solids compressibility along periods and groups, stressing the relevance of the valence average electron density. ELF turns out to be an important tool due to its ability to identify the pressure *controlling basin* and to quantify its charge and volume. All the data calculated so far correlate with the chemical concepts as classically established: it is always the valence electrons involved in the bond, the lone pair or the closed-shell basins that are responsible for the main compression within the systems, whereas cores remain practically untouched. Our study does not only confirm these principles but also endows them with a theoretical background, enabling the ability to foresee future behavior. Metals and pure covalent solids belong to a different class of materials than that of the rare-gas solids and molecular crystals, as far as the origin of their response to hydrostatic pressure is concerned. The stiffness in the two former kinds of solids is dominated by repulsive electrostatic interactions among the valence electrons (from one to three in metals, four in covalent solids) that increase as pressure is applied. For rare-gas solids and molecular crystals, it has been shown that only the outermost part of the lone pair basin suffers compression under pressure. This region starts from the most external maximum of the ELF and reflects the lack of homogeneity of the electron density within the lone pair basins. Pauli repulsions within closed-shell basins and between closed-shells of different ions or atoms prevent the different constituents of these systems from coming closer under pressure.

Acknowledgment. Financial support from the Spanish MEC and FEDER programs under project MAT2006-13548-C02-02 and the Spanish MALTA-Consolider Ingenio-2010 project CSD2007-00045 are gratefully acknowledged.

References

(1) Richards, T. W. *Proc. Natl. Acad. Sci. U.S.A.* **1915**, *1*, 411. Richards, T. W. *Proc. Natl. Acad. Sci. U.S.A.* **1923**, *9*, 73.

(2) Bridgman, P. W. *Proc. Natl. Acad. Sci. U.S.A.* **1922**, *8*, 361.

(3) Gilman, J. *Electronic Basis of the Strength of Materials*; Cambridge University Press: Cambridge, United Kingdom, 2003, pp 110−141.

(4) Becke, A. D.; Edgecombe, K. E. *J. Chem. Phys.* **1990**, *92*, 5397.

(5) Silvi, B.; Fourre, I.; Alikhani, E. *Monatshefte fur Chemie* **2005**, *136*, 855.

(6) Kresse, G.; Furthmuller, J. *Phys. Rev. B: Condens. Matter Mater. Phys.* **1996**, *54*, 11169.

(7) Saunders, V. R.; Dovesi, R.; Roetti, C.; Causá, M.; Harrison, N. M.; Orlando, R.; Zicovich-Wilson, C. M. *CRYSTAL98 User's Manual*; University of Torino: Torino, Italy, 1998.

(8) Noury, S.; Colonna, F.; Savin, A.; Silvi, B. *J. Mol. Struct.* **1998**, *450*, 59.

(9) Perdew, J. P.; Zunger, A. *Phys. Rev.* **1981**, *23*, 5048.

(10) Perdew, J. P.; Wang, Y. *Phys. Rev. B: Condens. Matter Mater. Phys.* **1992**, *45*, 13244.

(11) Towler, M., Crystal Resources Page, http://www.tcm.phy.cam.ac.uk/m̃dt26/crystal.html (accessed March 10, 2008).

(12) CRYSTAL Basis Sets Library, http://www.crystal.unito.it/Basis_Sets/ptable.html (accessed March 1, 2008).

(13) Otero de la Roza, A.; Blanco, M. A.; Martín Pendás, A.; Luaña, V. *Comput. Phys. Commun.* **2009**, *180*, 157.

(14) Contreras-García, J.; Martín Pendás, A.; Silvi, B.; Recio, J. M. *J. Phys. Chem. Solids* **2008**, *69*, 2204.

(15) Contreras-García, J.; Martín Pendás, A. M.; Recio, J. M. *J. Phys. Chem. B* **2008**, *112*, 9787.

(16) Contreras-García, J.; Silvi, B.; Martín Pendás, A. M.; Recio, J. M. *J. Phys. Chem. B* **2009**, *113*, 1068.

(17) Contreras-García, J.; Silvi, B.; Martín Pendás, A.; Recio, J. M. *J. Chem. Theory Comput.* **2009**, *5*, 164.

(18) Vinet, P.; Rose, J. H.; Ferrante, J.; Smith, J. R. *J. Phys.: Condens. Matter* **1989**, *1*, 1941.

(19) Martín Pendás, A.; Costales, A.; Blanco, M. A.; Recio, J. M.; Luaña, V. *Phys. Rev. B: Condens. Matter Mater. Phys.* **2000**, *62*, 13970.

(20) Recio, J. M.; Franco, R.; Martín Pendás, A.; Blanco, M. A.; Pueyo, L.; Pandey, R. *Phys. Rev. B: Condens. Matter Mater. Phys.* **2001**, *63*, 184101.

(21) Banerjea, A.; Smith, J. R. *Phys. Rev. B: Condens. Matter Mater. Phys.* **1988**, *37*, 6632.

(22) Rose, J. H.; Ferrante, J.; Smith, J. R. *Phys. Rev. Lett.* **1981**, *47*, 675.

(23) Martín Pendás, A.; Recio, J. M.; Francisco, E.; Luaña, V. *Phys. Rev. B: Condens. Matter Mater. Phys.* **1997**, *56*, 3010.

(24) Savin, A. *J. Chem. Sci.* **2005**, *117*, 473.

(25) Wu, B. R.; Sung, C. M.; Lee, S.-L.; Tai, M. F. *Chin. J. Phys.* **2002**, *40*, 187.

(26) Anderson, D. L.; Anderson, O. L. *J. Geophys. Res., [Atmos.]* **1970**, *75*, 3494.

(27) Hazen, R. M.; Finger, L. W. *J. Geophys. Res., [Atmos.]* **1979**, *84*, 6723.

(28) Waskowska, A.; Gerward, L.; Staun Olsen, J.; Feliz, M.; Llusar, R.; Gracia, L.; Marqués, M.; Recio, J. M. *J. Phys.: Condens. Matter* **2004**, *16*, 53.

(29) Kohout, M.; Savin, A. *Int. J. Quantum Chem.* **1996**, *60*, 875.

(30) Matito, E.; Silvi, B.; Duran, M.; Sola, M. *J. Chem. Phys.* **2006**, *125*, 024301.

CT900224W